This article has been accepted for publication in IEEE Transactions on Energy Conversion. This is the author's version which has not been fully edited and content may change prior to final publication. Citation information: DOI 10.1109/TEC.2023.3333530

Multiscale Finite Element Formulations for 2D/1D Problems

Karl Hollaus[1] and Markus Schöbinger[1]
[1]Technische Universität Wien, Institute for Analysis and Scientific Computing, A-1040 Vienna, Austria

Multiscale finite element methods for 2D/1D problems have been studied in this work to demonstrate their excellent ability to solve the eddy current problem in a single iron sheet of electrical machines. We believe that these methods are much more efficient than conventional 3D finite element methods and just as accurate. The 2D/1D multiscale finite element methods are based on a magnetic vector potential or a current vector potential. Known currents for excitation can be replaced by the Biot-Savart-field. Boundary conditions allow to integrate planes of symmetry. All approaches consider eddy currents, an insulation layer and preserve the edge effect. A segment of a fictitious electrical machine has been studied to demonstrate all above options, the accuracy and the low computational costs of the 2D/1D multiscale finite element methods. Numerous simulations are presented. Direct and iterative solvers were investigated to reliably solve the system of equations from 2D/1D MSFEMs.

***Index Terms*—Biot-Savart-field, direct solver, eddy currents, edge effect, iterative solver, thin iron sheets, 2D/1D multiscale finite element method MSFEM**

I. Introduction

THE overall dimensions of a laminated core of electrical machines are essentially larger than the thickness of a single iron sheet and thus such machines represent a multiscale problem. Neglecting the magnetic stray fields at the end region, all iron sheets are exposed to roughly the same field distribution. Thus, a simulation of a single sheet instead of the whole core suffices.

The brute force way is to exploit three-dimensional (3D) finite element methods (FEMs) for the single sheet. However, simulations with 3D FEMs may still become too expensive for routine tasks [1].
A very efficient approach is the use of an effective material with a complex-valued magnetization curve [2]. However, methods with an effective material are restricted to problems in the steady state.
Attractive alternative options to 3D FEMs are space splitting two-dimensional/one-dimensional (2D/1D) methods, see for instance [3], [4] and [5]. To take account of the eddy currents a 1D diffusion equation is solved. These methods suffer from a high number of subdivisions along the thickness of the sheet.
Methods with an effective material and the 2D/1D methods ignore the edge effect (EE), i.e. the closure paths of the eddy currents are neglected, see [6] and [7]. The EE is particularly important, for instance, in the tooth tips which are exposed to high flux variations ([1]) and because of the degrading effect due to the cutting process of iron sheets, see for example [8], [9] and [10].

Therefore, the idea is to replace the 3D FEMs and

Manuscript received Oct 26, 2022; revised xxx, xx. Corresponding author: K. Hollaus (email: karl.hollaus@tuwien.ac.at)

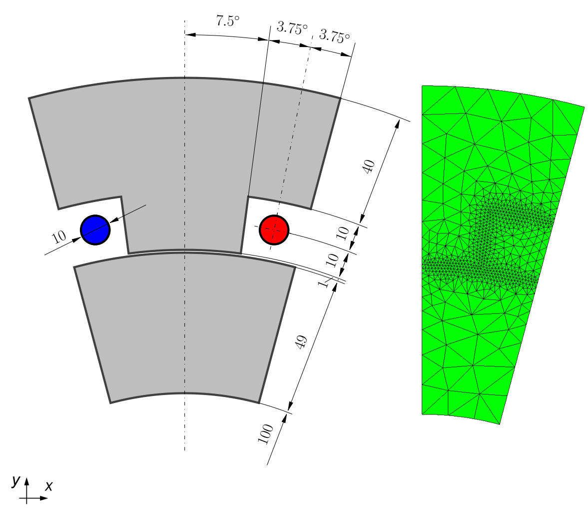

Fig. 1. The segment is a twelfth of a fictitious electrical machine (left) with a rotor and a stator separated by an air gap and assumed to be in the xy-plane. Dimensions are in mm. Thickness of the iron sheets is d=0.5mm. Known opposed currents in conductors with circular cross-section represent the excitation. Finite element mesh of one half of the segment (right).

the 2D/1D methods by 2D/1D MSFEMs based on a magnetic vector potential (MVP) $\boldsymbol{A}$ or a current vector potential (CVP) $\boldsymbol{T}$-formulation. The 2D/1D multiscale finite element methods (MSFEMs) need only a 2D finite element (FE) mesh. This leads to much less unknowns in the FE system of equations. The FE system matrix is much sparser than in 3D FEMs. All this results in a drastic reduction of computational costs, both memory requirements and computational times. The 2D/1D MSFEMs significantly reduce the overhead of the earlier

This article has been accepted for publication in IEEE Transactions on Energy Conversion. This is the author's version which has not been fully edited and content may change prior to final publication. Citation information: DOI 10.1109/TEC.2023.3333530

2D/1D methods. The versatility of 2D/1D MSFEMs is that of 3D FEMs for a sheet.
A 2D/1D MSFEM using trigonometric functions across the thickness of the sheet can be found in [11]. Our methods also have to consider eddy currents including the EE, see [7], account for an insulation layer in between the iron sheets, facilitate boundary conditions (BCs) to exploit planes of symmetry, and use Biot-Savart-fields (BSF) to avoid modeling of conductors carrying known currents. So far, an excitation has been introduced only by proper BCs in the tiny problem in [12] and [7].

A small part of the work was presented at CEFC 2022 [13]. First, the basic eddy current problem (ECP) with BCs is presented in Sec. II. The segment of a fictitious electric machine in Fig. 1 serves as model problem. For the sake of simplicity linear material relations and steady state are assumed, thus the work is carried out in the frequency domain. Nevertheless all advantages of 2D/1D MSFEMs over 3D FEM can be shown. Then, four 2D/1D MSFEM approaches are introduced in Sec. III. A motivation of the construction, various properties, boundary conditions in detail and FE approximation of the 2D/1D MSFEMs can be found in Secs. III-A, III-B, III-C and III-D, respectively. In contrast to [12] and [7], the new approaches (17) and (20) use either $H(\mathrm{curl})$ or H^1 finite element spaces. To evaluate the accuracy and efficiency of the 2D/1D MSFEMs, mixed FEMs have been used which are briefly described in Sec. IV. Simulation results obtained by the 2D/1D MSFEMs by means of the numerical example in Fig. 1 are presented in Sec. V. The accuracy of the 2D/1D MSFEMs is shown in terms field and specific loss distributions in Sec. V-C and by EC losses in Sec. V-D. To show the computational cost, the required unknowns, non-zero entries in the system matrix, and computational times are presented in Sec. V-E. The ability of 2D/1D MSFEMs to handle small penetration depths is investigated in terms of frequency sweeps in Sec. V-F. The accuracy of modeling the EE by $\boldsymbol{A}$- and $\boldsymbol{T}$-formulations has also been studied in the previous mentioned sections.

In summary, the 2D/1D MSFEMs show high accuracy, comparable to the expensive 3D FEMs, but require very low computational cost.

II. Eddy Current Problem

An ECP has to be solved, see Fig. 1. The entire domain $\Omega = \Omega_c \cup \Omega_0 \subset \mathbb{R}^3$ consists of the conducting domain (iron sheets) Ω_c and the nonconducting domain (air or insulation layer) Ω_0, compare with Fig. 2. The normal vector $\boldsymbol{n}$ points out of Ω and Ω_c, respectively. To facilitate the representation of the ECP the following definitions are introduced

$$\Gamma_H = \Gamma_r \quad (1)$$

$$\Gamma_J = \Gamma_{ic} \cup \Gamma_{rc} \cup \Gamma_{gc} \cup \Gamma_{oc} \cup \Gamma_{bc} \cup \Gamma_{tc}, \quad (2)$$

$$\Gamma_B = \Gamma_i \cup \Gamma_o \cup \Gamma_l \cup \Gamma_b \cup \Gamma_t, \quad (3)$$

$$\Gamma_E = \Gamma_{lc}. \quad (4)$$

The additional index c means the part of the respective boundary connected with a conductive domain. The ECP

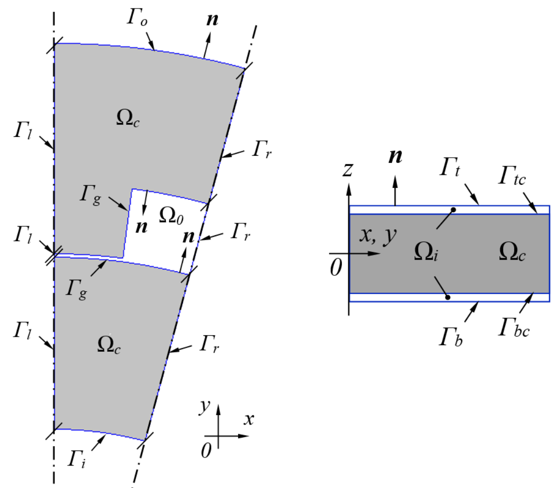

Fig. 2. One half of the segment in the xy-plane (left), iron sheet in grey. Detail of the cross-section with iron sheet and with half a layer of insulation on top and half on the bottom (right), not to scale.

consists of a quasi-static magnetic field

$$\mathrm{curl}\,\boldsymbol{H} = \boldsymbol{J}, \quad (5)$$

$$\mathrm{curl}\,\boldsymbol{E} = -j\omega\boldsymbol{B}, \quad (6)$$

$$\mathrm{div}\,\boldsymbol{B} = 0 \quad (7)$$

with

$$\boldsymbol{J} = \sigma\boldsymbol{E} \text{ or } \boldsymbol{E} = \rho\boldsymbol{J}, \boldsymbol{B} = \mu\boldsymbol{H} \text{ or } \boldsymbol{H} = \nu\boldsymbol{B} \quad (8)$$

in Ω_c and a static magnetic field

$$\mathrm{curl}\,\boldsymbol{H} = \boldsymbol{J}_0, \quad (9)$$

$$\mathrm{div}\,\boldsymbol{B} = 0 \quad (10)$$

with

$$\boldsymbol{B} = \mu_0\boldsymbol{H} \text{ or } \boldsymbol{H} = \nu_0\boldsymbol{B} \quad (11)$$

in Ω_0 and the BCs

$$\boldsymbol{H} \times \boldsymbol{n} = \boldsymbol{0} \quad \text{on } \Gamma_H, \quad (12)$$

$$\boldsymbol{J} \cdot \boldsymbol{n} = 0 \quad \text{on } \Gamma_J, \quad (13)$$

$$\boldsymbol{B} \cdot \boldsymbol{n} = 0 \quad \text{on } \Gamma_B, \quad (14)$$

$$\boldsymbol{E} \times \boldsymbol{n} = \boldsymbol{0} \quad \text{on } \Gamma_E, \quad (15)$$

where $\boldsymbol{H}$ is the magnetic field strength, $\boldsymbol{J}$ the electric current density, $\boldsymbol{E}$ the electric field strength, $\boldsymbol{B}$ the magnetic flux density, σ the electric conductivity, ρ the electric resistivity, μ the magnetic permeability, ν the magnetic reluctivity and $\boldsymbol{J}_0$ the prescribed electric current density, respectively, j denotes the imaginary unit and ω the angular frequency. Since there is only the magnetic field in the entire domain Ω, the continuity conditions on the interface Γ_{c0} between Ω_c and Ω_0 are

$$\boldsymbol{H} \times \boldsymbol{n} \text{ and } \boldsymbol{B} \cdot \boldsymbol{n} \tag{16}$$

which are continuous.

If the symmetry in the segment is not used, Γ_l does not exist. In the considered example, the BC $\boldsymbol{B} \cdot \boldsymbol{n} = 0$ on $\Gamma_i \cup \Gamma_o$ represents a simplification and is in reality only approximately fulfilled and on $\Gamma_b \cup \Gamma_t$ an assumption that no magnetic stray field exists.

III. 2D/1D MSFEM Formulations

The entire domain $\Omega = \Omega_m \cup \Omega_0 \subset \mathbb{R}^2$ is composed of a laminated domain $\Omega_m = \Omega_c \cup \Omega_i$ representing an iron sheet and half an insulation layer on each side of the sheet, compare with the detail in Fig. 2, and the non-conducting domain Ω_0 representing the air gap between the rotor and the stator and the space for conductors with known currents, see also Fig. 1. Note that the meaning of Ω_m and Ω_0 depends on the context, either that of a 2D/1D MSFEM or that of the reference solution.

A. 2D/1D MSFEM Approaches

The considered MSFEMs approaches

$$\widetilde{\boldsymbol{T}}_1 = \boldsymbol{T}_0 + \phi_2 \boldsymbol{T}_2 + \boldsymbol{H}_{BS} \tag{17}$$

$$\widetilde{\boldsymbol{T}}_2 = \operatorname{grad} \Phi_0 + \phi_2 \boldsymbol{T}_2 + \boldsymbol{H}_{BS} \tag{18}$$

$$\widetilde{\boldsymbol{A}}_1 = \phi_1^0 \operatorname{grad} u_{10} + \phi_1 \boldsymbol{A}_1 + \operatorname{grad}(\phi_1 w_1) \tag{19}$$

$$\widetilde{\boldsymbol{A}}_2 = \phi_1^0 \operatorname{grad} u_{10} + \phi_1 \operatorname{grad} u_1 + \phi_{1,z}(0,0,w_1)^T \tag{20}$$

are denoted by a tilde, where $\boldsymbol{H}_{BS}$ stands for the Biot-Savart field. The approaches (17) to (20) are denoted by TMS1, TMS2, AMS1 and AMS2, respectively. The potentials $\boldsymbol{T}_0$, $\boldsymbol{T}_2$, Φ_0, u_{10}, $\boldsymbol{A}_1$, w_1 and u_1, respectively, are unknown and depend on x and y, for example $\boldsymbol{T}_0 = \boldsymbol{T}_0(x, y)$. The dependence on the z-direction is modeled by the micro-shape functions (MSFs) shown in Fig. 3. The multiplication of a coefficient function or its derivative by a micro-shape function or its derivative leads to the space-splitting approaches (17) to (20).

The MSFs ϕ_1, ϕ_2 and ϕ_1^0, where $\phi_{1,z}$ is the derivative of ϕ_1 with respect to z are shown in Fig. 3.
Figure 3 shows how the MSFs fit into the periodic structure with $p = d + d_i$, where d is the thickness of the iron sheet and d_i that of the insulation layer. The polynomials

$$\phi_1(s) = s, \quad \phi_2(s) = \frac{1}{2}\sqrt{\frac{3}{2}}(s^2 - 1) \tag{21}$$

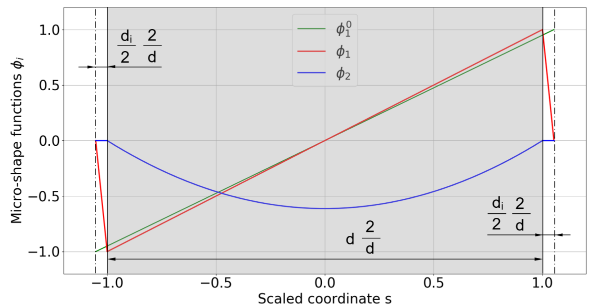

Fig. 3. Micro-shape functions ϕ_i: The gray interval [-1, 1] represents the thickness of the iron sheet, and beyond that up to the dashed–dotted line, there is the insulation layer.

are used as MSFs with the mapping $s = 2z/d$, where $s \in [-1, 1]$ and $z \in [-d/2, d/2]$. The MSFs ϕ_1^0 is linear and becomes ± 1 on the boundary $\Gamma_z = \{-(d + d_i)/2, (d+d_i)/2\}$, ϕ_1 is piecewise linear and 0 on Γ_z and ϕ_2 is zero on $[-(d+d_i)/2, -d/2)$ and $(d/2, (d+d_i)/2]$ which corresponds to the insulation layer. These polynomials facilitate the required tangential continuity of the unknowns in the multiscale approaches and ϕ_1^0 allows to prescribe essential BCs. The required symmetry of the solution with respect to $z = 0$, is ensured by selecting either even or odd MSFs in the 2D/1D MSFEM approaches explicitly.

The approaches (17) to (20) consist basically of three terms. To explain their meaning, think of the magnetic field strength $\boldsymbol{H}$ and flux density $\boldsymbol{B}$ for TMS1 and TMS2 and on the electric field strength $\boldsymbol{E}$ and current density $\boldsymbol{J}$ for AMS1 and AMS2, respectively, and on the other on the analytic solution of a 1D eddy current flow in an infinite slab derived for example in [14]. Apart from the EE, a suitable approach for TMS1 and TMS2 must be an even function and for AMS1 and AMS2 an odd function along the sheet thickness, with the middle of the sheet serving as the origin.

The first term $\boldsymbol{T}_0$ or $\operatorname{grad} \Phi_0$ of TMS1 and TMS2 provides an average magnetic flux density across p, the thickness of the sheet including the insulation layer, which is corrected by the second term $\phi_2 \boldsymbol{T}_2$ to account for penetration depth. The EE is simply modeled by homogenous tangential BCs for $\boldsymbol{T}_2$ on respective boundaries. Similarly, for AMS1 and AMS2, the circulation of $\phi_1^0 \operatorname{grad} u_{10}$ yields a constant flux density across p. A partitioning of the magnetic flux between iron and insulation layer is accomplished by the circulation of the second term $\phi_1 \boldsymbol{A}_1$ or $\phi_1 \operatorname{grad} u_1$. The third terms $\operatorname{grad}(\phi_1 w_1)$ in (19) or $\phi_{1,z}(0,0,w_1)^T$ in (20) represent the EE.

This article has been accepted for publication in IEEE Transactions on Energy Conversion. This is the author's version which has not been fully edited and content may change prior to final publication. Citation information: DOI 10.1109/TEC.2023.3333530

B. Properties of the MSFEM Formulations

In order to facilitate the discussion of the 2D/1D MSFEM approaches and to find the true BCs more easily some intermediate results are presented:

$$\operatorname{curl} \boldsymbol{T}_0 = \begin{pmatrix} 0 \\ 0 \\ T_{0y,x} - T_{0x,y} \end{pmatrix} \quad (22)$$

$$\operatorname{curl}(\phi_2 \boldsymbol{T}_2) = \begin{pmatrix} -\phi_{2,z} T_{2y} \\ \phi_{2,z} T_{2x} \\ \phi_2 (T_{2y,x} - T_{2x,y}) \end{pmatrix} \quad (23)$$

$$\operatorname{curl} \boldsymbol{H}_{BS} = \boldsymbol{J}_0 \quad (24)$$

$$\operatorname{curl}(\phi_1^0 \operatorname{grad} u_{10}) = \begin{pmatrix} -\phi_{1,z}^0 u_{10,y} \\ \phi_{1,z}^0 u_{10,x} \\ 0 \end{pmatrix} \quad (25)$$

$$\operatorname{curl}(\phi_1 \boldsymbol{A}_1) = \begin{pmatrix} -\phi_{1,z} A_{1y} \\ \phi_{1,z} A_{1x} \\ \phi_1 (A_{1y,x} - A_{1x,y}) \end{pmatrix} \quad (26)$$

$$\operatorname{curl}(\phi_1 \operatorname{grad} u_1) = \begin{pmatrix} -\phi_{1,z} u_{1,y} \\ \phi_{1,z} u_{1,x} \\ 0 \end{pmatrix} \quad (27)$$

$$\operatorname{curl}(0, 0, \phi_{1,z} w_1) = \begin{pmatrix} \phi_{1,z} w_{1,y} \\ -\phi_{1,z} w_{1,x} \\ 0 \end{pmatrix} \quad (28)$$

Magnetic fields that occur in air are represented by $\boldsymbol{T}_0$ in (17). As can be seen in (23) the term $\phi_2 \boldsymbol{T}_2$ is essential for the $\boldsymbol{T}$-formulations (17) and (18) to get proper eddy current density distributions. Setting the trace of $\boldsymbol{T}_2$ to zero yields the component for the EE $J_z = \phi_2(T_{2y,x} - T_{2x,y})$. The other components J_x and J_y vanish, compare with (23). This is a big advantage over the $\boldsymbol{A}$-formulations (19) and (20), which additionally require a third term. To preserve the EE, $\phi_2 \boldsymbol{T}_2$ can not be replaced by a term like $\phi_2 \operatorname{grad}(u_2)$, because $\operatorname{curl}(\phi_2 \operatorname{grad}(u_2))$ does not have a z-component. In case of $\boldsymbol{A}$-formulations the EE is represented by $\operatorname{grad}(\phi_1 w_1)$ and by $\phi_{1,z}(0, 0, w_1)^T$ in (19) and (20), respectively. Laminar currents due to $\phi_1^0 \operatorname{grad} u_{10}$ generate a total magnetic flux (25), which is perturbed either by (26), see [7], or by (27). The z-component of $\operatorname{curl}(\phi_1 \boldsymbol{A}_1)$ provides a smoothing of the magnetic field at the transition from the iron sheet to the air. While the z-component of the current density due to $\phi_{1,z} w_1$ is accompanied by the magnetic field (28), $\operatorname{grad}(\phi_1 w_1)$ does not yield a magnetic field.

Known total source currents in conductors pointing in z-direction and considering a penetration depth could be simply prescribed by $\boldsymbol{T}_0$. On the other hand, a magnetic flux density, for example, in an air gap of an electric machine could be simply represented by $\operatorname{grad} \Phi_0$ or $\phi_1^0 \operatorname{grad} u_{10}$. The main magnetic flux, which is parallel to the iron sheet, is considered by all approaches and causes eddy currents confined to flow in very narrow loops.

C. Boundary Conditions of the 2D/1D MSFEMs

To fulfill the BCs (12) to (15) for the problem in Fig. 2 by the methods (17) to (20) their potentials $\boldsymbol{T}_0$, $\boldsymbol{T}_2$, u_{10}, $\boldsymbol{A}_1$, u_1 and w_1 must be specified as follows. Other used boundaries here are

$$\Gamma_{J_{2D}} = \Gamma_i \cup \Gamma_r \cup \Gamma_o \cup \Gamma_g, \quad (29)$$

$$\Gamma_{B_{2D}} = \Gamma_l \cup \Gamma_i \cup \Gamma_o. \quad (30)$$

1) TMS1

$$\boldsymbol{T}_0 \times \boldsymbol{n} = \boldsymbol{0} \quad \text{on } \Gamma_H \quad (31)$$

$$\boldsymbol{T}_2 \times \boldsymbol{n} = \boldsymbol{0} \quad \text{on } \Gamma_{J_{2D}} \quad (32)$$

$$-j\omega\mu \widetilde{\boldsymbol{T}}_1 \cdot \boldsymbol{n} = 0 \quad \text{on } \Gamma_{B_{2D}} \quad (33)$$

$$\rho \operatorname{curl}(\boldsymbol{T}_0 + \Phi_2 \boldsymbol{T}_2) \times \boldsymbol{n} = \boldsymbol{0} \quad \text{on } \Gamma_E \quad (34)$$

2) TMS2

$$\Phi_0 = 0 \quad \text{on } \Gamma_H \quad (35)$$

$$\boldsymbol{T}_2 \times \boldsymbol{n} = \boldsymbol{0} \quad \text{on } \Gamma_{J_{2D}} \quad (36)$$

$$-j\omega\mu \widetilde{\boldsymbol{T}}_2 \cdot \boldsymbol{n} = 0 \quad \text{on } \Gamma_{B_{2D}} \quad (37)$$

$$\rho \operatorname{curl}(\Phi_2 \boldsymbol{T}_2) \times \boldsymbol{n} = \boldsymbol{0} \quad \text{on } \Gamma_E \quad (38)$$

3) AMS1

$$\nu \operatorname{curl}(\widetilde{\boldsymbol{A}}_1) \times \boldsymbol{n} = \boldsymbol{0} \quad \text{on } \Gamma_H \quad (39)$$

$$-j\omega\sigma \widetilde{\boldsymbol{A}}_1 \cdot \boldsymbol{n} = 0 \quad \text{on } \Gamma_{J_{2D}} \quad (40)$$

$$u_{10} = 0, \quad (41)$$

$$w_1 = 0, \quad (42)$$

$$\boldsymbol{A}_1 \times \boldsymbol{n} = \boldsymbol{0} \quad \text{on } \Gamma_{B_{2D}} \quad (43)$$

4) AMS2

$$\nu \operatorname{curl}(\widetilde{\boldsymbol{A}}_2) \times \boldsymbol{n} = \boldsymbol{0} \quad \text{on } \Gamma_H \quad (44)$$

$$-j\omega\sigma \widetilde{\boldsymbol{A}}_2 \cdot \boldsymbol{n} = 0 \quad \text{on } \Gamma_{J_{2D}} \quad (45)$$

$$u_{10} = 0, \quad (46)$$

$$u_1 = 0, \quad (47)$$

$$w_1 = 0 \quad \text{on } \Gamma_{B_{2D}} \quad (48)$$

D. Finite Element Approximation

To obtain the respective weak form of the 2D/1D MSFEMs approaches, (17) to (20) are substituted into one of the partial differential equations

$$\operatorname{curl}(\rho \operatorname{curl} \widetilde{\boldsymbol{T}}) + j\omega\mu \widetilde{\boldsymbol{T}} = \boldsymbol{0} \text{ or} \quad (49)$$

$$\operatorname{curl}(\nu \operatorname{curl} \widetilde{\boldsymbol{A}}) + j\omega\sigma \widetilde{\boldsymbol{A}} = \boldsymbol{J}_0 \quad (50)$$

and known steps considering the BCs (31) to (48) are carried out for the FEM ([12], [7], [6]).

Finite element subspaces of the potentials have been

This article has been accepted for publication in IEEE Transactions on Energy Conversion. This is the author's version which has not been fully edited and content may change prior to final publication. Citation information: DOI 10.1109/TEC.2023.3333530

TABLE I
ORDER OF THE METHODS FEO AND THEIR POTENTIALS

FEO		0	1	2
$\boldsymbol{T}$,Φ-Φ	$\boldsymbol{T}$	0	1	2
	Φ	1	2	3
TMS1	$\boldsymbol{T}_0$	0	1	2
	$\boldsymbol{T}_2$	0	1	2
TMS2	Φ_0	1	2	3
	$\boldsymbol{T}_2$	0	1	2
$\boldsymbol{A}$,V-$\boldsymbol{A}$	$\boldsymbol{A}$	0	1	2
	V	1	2	3
AMS1	u_{10}	1	2	3
	$\boldsymbol{A}_1$	0	1	2
	w_1	1	2	3
AMS2	u_{10}	1	2	3
	u_1	1	2	3
	w_1	1	1	2

selected as follows: $\boldsymbol{T}_0 \in H(\mathrm{curl}, \Omega)$, $\boldsymbol{T}_2$ and $\boldsymbol{A}_1 \in H(\mathrm{curl}, \Omega_m)$, Φ_0 and $u_{10} \in H^1(\Omega)$ and u_1 and $w_1 \in H^1(\Omega_m)$, see [15]. The MSFs are in the space of periodic and continuous functions $H_{per}([-p/2, p/2])$.

Following the usual designations, we call $H(\mathrm{curl})$ conforming FEs edge elements and H^1 conforming FEs nodal elements. The FE order (FEO) refers to edge elements for $\boldsymbol{T}_0$, $\boldsymbol{T}_2$ and $\boldsymbol{A}_1$, compare with Tab. I. The FEO of nodal elements for Φ_0, u_{10}, u_1 and w_1 in (19) is one higher than that of the edge elements for $\boldsymbol{T}_0$, $\boldsymbol{T}_2$, $\boldsymbol{A}_1$, $\boldsymbol{T}$ and $\boldsymbol{A}$ to be consistent with the de-Rham-complex. An exception is w_1 in (20) with the same order as the edge elements. MSFEM approach (17) uses only edge elements and (20) only nodal elements.

The weak forms have been derived as described for example in [6], [12] and [16] for a MSFEM based on a MVP and in [12] and [17] for a MSFEM based on a CVP. Averaging of the coefficients in the bilinear forms has been carried out to exploit the advantage of the MSFEMs, see [6] and [12]. Since the material properties are assumed to be linear, averaging of the coefficients in z-direction can be carried out analytically. Therefore, averaging does not effect the FE mesh in the xy-plane.

The BSF $\boldsymbol{H}_{BS}$ is included into the approaches (17) and (18) based on a CVP. In case of approaches based on a MVP the known current density $\boldsymbol{J}_0$ is directly considered on the right hand side in the corresponding linear form of the MSFEM and integration by parts.

IV. REFERENCE SOLUTIONS

Reference solutions have been computed using the mixed formulations $\boldsymbol{A}, V$-$\boldsymbol{A}$ and $\boldsymbol{T}$, Φ-Φ ([18]), where V is the electric scalar potential and Φ the magnetic scalar potential, and with 3D FE models with second order FEs of the entire segment in Fig. 1, see also Tab. I. Only mixed formulations, e.g. $\boldsymbol{T}$, Φ-Φ and $\boldsymbol{A}, V$-$\boldsymbol{A}$, allow the modeling of all BCs of the considered specific problem. For example, the representation of the BC in (2) on Γ_o is not possible using only $\boldsymbol{A}$.

1) Boundary Value Problem with $\mathbf{T}$,Φ-Φ

$$\begin{aligned} &\mathrm{curl}\, \rho\, \mathrm{curl}\, \boldsymbol{T} + j\omega\mu(\boldsymbol{T} - \mathrm{grad}\, \Phi) \\ &= -\,\mathrm{curl}\, \rho\, \mathrm{curl}\, \boldsymbol{H}_{BS} - j\omega\mu \boldsymbol{H}_{BS}, \end{aligned} \tag{51}$$

$$j\omega\, \mathrm{div}(\mu(\boldsymbol{T} - \mathrm{grad}\, \Phi)) = -j\omega\, \mathrm{div}(\mu \boldsymbol{H}_{BS}) \quad \text{on } \Omega_c \tag{52}$$

$$-j\omega\, \mathrm{div}(\mu_0\, \mathrm{grad}\, \Phi) = -j\omega\, \mathrm{div}(\mu_0 \boldsymbol{H}_{BS}) \quad \text{on } \Omega_0 \tag{53}$$

$$\boldsymbol{T} \times \boldsymbol{n} = \boldsymbol{0}, \tag{54}$$

$$\Phi = 0 \quad \text{on } \Gamma_H \tag{55}$$

$$\boldsymbol{T} \times \boldsymbol{n} = 0 \quad \text{on } \Gamma_J \tag{56}$$

$$-j\omega\mu(\boldsymbol{T} + \boldsymbol{H}_{BS} - \mathrm{grad}\, \Phi) \cdot \boldsymbol{n} = 0 \quad \text{on } \Gamma_B \tag{57}$$

$$\rho\, \mathrm{curl}\, \boldsymbol{T} \times \boldsymbol{n} = \boldsymbol{0} \quad \text{on } \Gamma_E \tag{58}$$

2) Boundary Value Problem with $\mathbf{A}$,V-$\mathbf{A}$

$$\mathrm{curl}\, \nu\, \mathrm{curl}\, \boldsymbol{A} + j\omega\sigma(\boldsymbol{A} + \mathrm{grad}\, V) = \boldsymbol{0}, \tag{59}$$

$$\mathrm{div}(j\omega\sigma(\boldsymbol{A} + \mathrm{grad}\, V)) = 0 \quad \text{on } \Omega_c \tag{60}$$

$$\mathrm{curl}\, \nu_0\, \mathrm{curl}\, \boldsymbol{A} = \boldsymbol{J}_0 \quad \text{on } \Omega_0 \tag{61}$$

$$\nu\, \mathrm{curl}\, \boldsymbol{A} \times \boldsymbol{n} = \boldsymbol{0} \quad \text{on } \Gamma_H \tag{62}$$

$$-j\omega\sigma(\boldsymbol{A} + \mathrm{grad}\, V) \cdot \boldsymbol{n} = 0 \quad \text{on } \Gamma_J \tag{63}$$

$$\boldsymbol{A} \times \boldsymbol{n} = \boldsymbol{0} \quad \text{on } \Gamma_B \tag{64}$$

$$V = 0, \tag{65}$$

$$\boldsymbol{A} \times \boldsymbol{n} = \boldsymbol{0} \quad \text{on } \Gamma_E \tag{66}$$

Details of the associated weak forms can be found, for example, in [18].

V. NUMERICAL SIMULATIONS

A. Problem

The problem is a segment of a fictitious electrical machine shown with details in Fig. 1. A conductivity of $\sigma = 2.08 \cdot 10^6 \mathrm{S/m}$, a relative permeability of $\mu_r = 1,000$, a frequency of $f = 50\mathrm{Hz}$, a thickness of the sheet of $d = 0.5\mathrm{mm}$, a fill factor of $k_f = 0.95$ and a peak value of the current $I = 100\mathrm{A}$ have been selected. The BSF fulfills the rotational symmetry due to the prescribed currents (24), half of which point into the opposite direction.

B. Results

For the sake of a fair comparison the FE mesh for the 3D FEM has been generated by extrusion of the 2D mesh for the 2D/1D MSFEMs with prism-shaped elements. The 3D FEM models consist of six layers of elements with proper thicknesses to account for the penetration depth.

All methods have been implemented in Netgen/NGSolve [19] and all problems have been solved by the direct solver PARDISO [20].

This article has been accepted for publication in IEEE Transactions on Energy Conversion. This is the author's version which has not been fully edited and content may change prior to final publication. Citation information: DOI 10.1109/TEC.2023.3333530

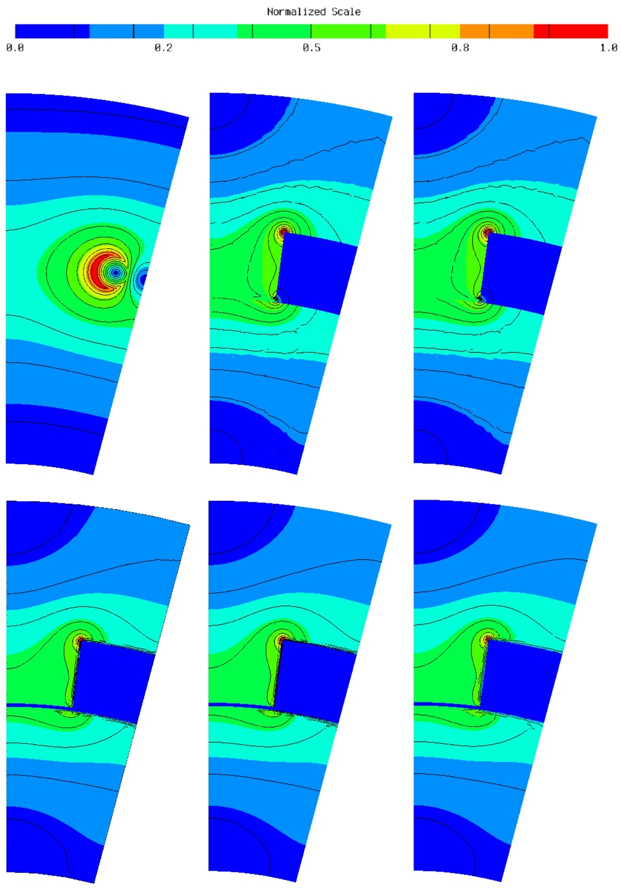

Fig. 4. Top: Biot-Savart-field $|\boldsymbol{H}_{BS}|$ to the left ($|\boldsymbol{H}_{BS}|_{max} = 3,779\text{kA/m}$), magnetic flux density $|\boldsymbol{B}|$ of $\mathbf{T}$,Φ-Φ in the middle and of TMS1 to the right ($|\boldsymbol{B}|_{max} = 0.273\text{T}$), all at z=0. Bottom: Current density $|\boldsymbol{J}|$ ($|\boldsymbol{J}|_{max} = 35\text{kA/m}^2$) of $\mathbf{A}$,V-$\mathbf{A}$ to the left, of AMS1 in the middle and of AMS2 to the right, all at z=0.188mm and with FEO=2 (see Tab. I). The black contours are isolines.

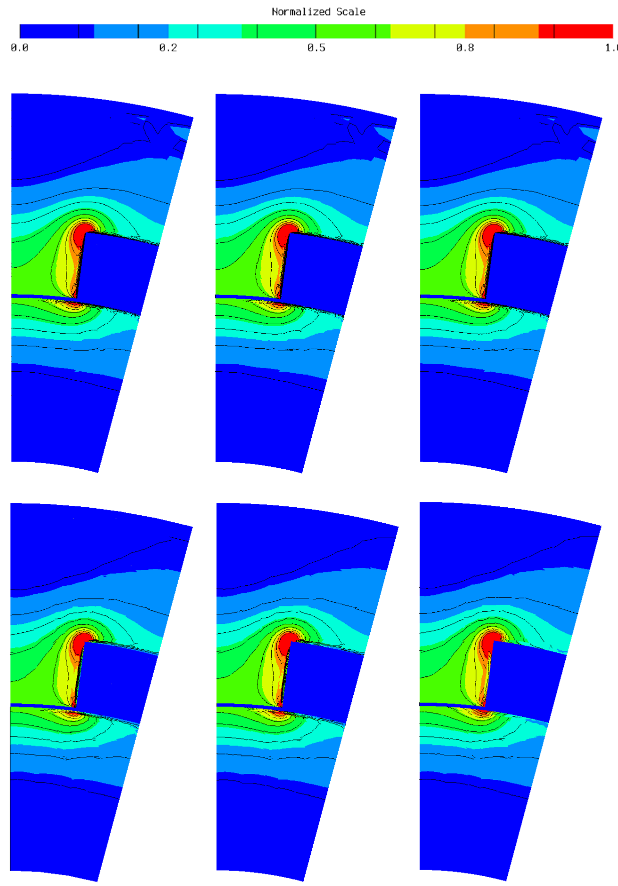

Fig. 5. Specific losses p in W/m^3, range is $0 < p < 100\text{W/m}^3$. Top: $\mathbf{T}$,Φ-Φ to the left, TMS1 in the middle and TMS2 to the right. Bottom: $\mathbf{A}$,V-$\mathbf{A}$ to the left, TMS1 in the middle and TMS2 to the right. All at z=0.188mm and with FEO=2 (see Tab. I). The black contours are isolines.

C. Field and Specific Loss Distribution

For comparison, the field and specific loss distributions in the xy-plane at z=0.188mm are shown in Fig. 4 and Fig. 5. The EC density distribution in the xz-plane at y=0.153m is shown in Fig. 6. There is a very satisfactory agreement in all cases.

D. Eddy Current Losses

The reference solutions for these losses were computed by $\boldsymbol{T}, \Phi$-Φ for TMS1 and TMS2, respectively, and by $\boldsymbol{A}, V$-$\boldsymbol{A}$ for AMS1 and AMS2, respectively, with 3D FE models of the entire segment in Fig. 1 with second order FEs FEO=2. An evaluation of the overall EC losses of the half problem by means of the relative error

$$RE = \frac{2P_{2D/1D} - P_{3D}}{P_{3D}} \cdot 100\% \tag{67}$$

are shown in Fig. 7. The reference losses P_{3D} of the entire problem are summarized in Tab. II, $P_{2D/1D}$ are

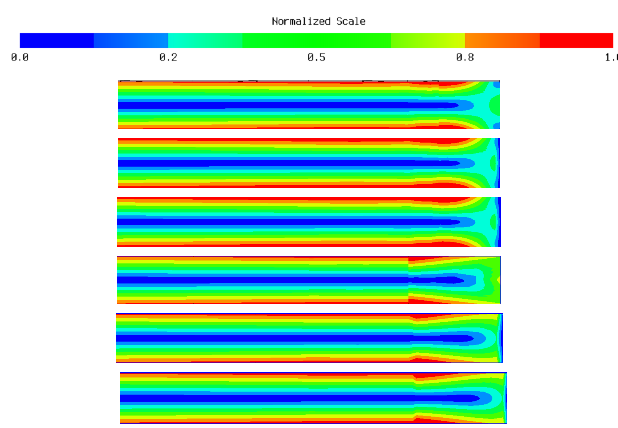

Fig. 6. Distribution of the eddy current density $|\mathbf{J}|$ in A/m^2, range is $0 < |\mathbf{J}| < 2.5 \cdot 10^4\text{A/m}^2$, detail of cross section at $y = 0.153\text{m}$ (compare with Fig. 1). From the top to the bottom: $\mathbf{T}$,Φ-Φ, TMS1, TMS2, $\mathbf{A}$,V-$\mathbf{A}$, AMS1, AMS2. All with FEO=2 (see Tab. I).

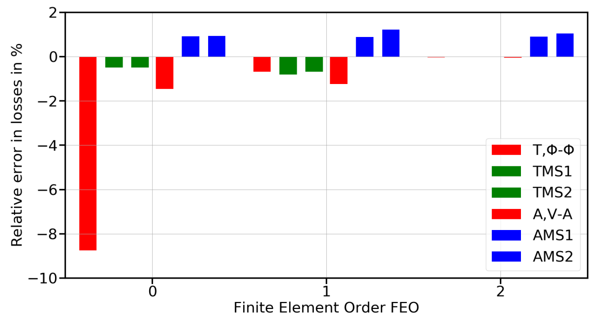

Fig. 7. Relative error of eddy current losses.

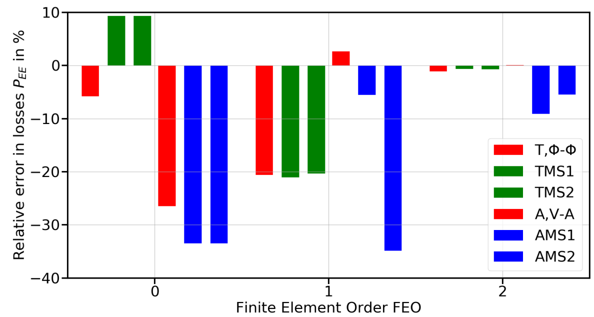

Fig. 8. Relative error of losses P_{EE} according to (68).

the losses obtained by 2D/1D MSFEMs of the half problem. Thus, the relative error RE includes also the ability of the 2D/1D MSFEMs to model the symmetry of the problem. The relatively large error for lowest order $\boldsymbol{T}, \Phi$-Φ can be explained by the fact that the current density $\boldsymbol{J}$ is the circulation of the CVP $\operatorname{curl} \boldsymbol{T}$ being just piecewise constant with lowest order edge elements. The high accuracy of 2D/1D MSFEMs with zero order FEs is due to the local description of the solution using MSFs. The RE is negligible small for TMS1 and TMS2 and second order FEs. However, the RE is about 1% for AMS1 and AMS2 independent of the FEO. Simply speaking, this indicates that the formulations of AMS1 and AMS2 are less suitable.

The capability to represent the EE by the 2D/1D MSFEMs is presented in Fig. 8. The normal component, i.e. the z-component, of the current density represents the so-called EE. The EE is not present in the plane of symmetry Γ_l. The losses

$$P_{EE} = 0.5 \int_{\Omega_c} \sigma^{-1} J_z J_z^* \, d\Omega, \tag{68}$$

where J_z is the z-component of the current density and $*$ means conjugate complex, have been computed as a measure to study the capability to consider the EE by the 2D/1D MSFEMs. The REs on P_{EE} are defined analogously to (67) and were calculated for TMS1 and TMS2 with respect to the reference solutions (51) to (58) and those for AMS1 and AMS2 with (59) to (66). The RE of the EE practically vanishes for TMS1 and TMS2 with second order FEs FEO=2, whereas it stays relatively large for AMS1 and AMS2, as can be seen in Fig. 8. Modeling of the EE requires just a homogenous

TABLE II
EDDY CURRENT LOSSES

Formulation	$\boldsymbol{T}, \Phi$-Φ	$\boldsymbol{A}, V$-$\boldsymbol{A}$
P in μW	47.65	47.40

Second order FEs FEO=2, see Tab. I, entire problem.

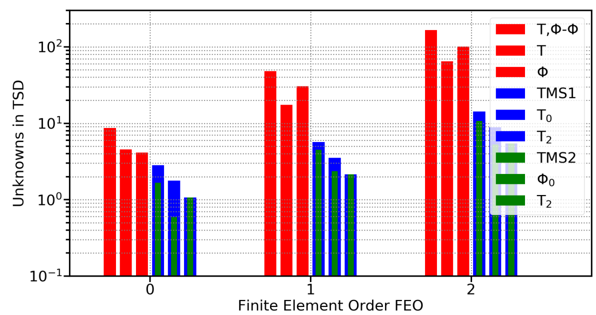

Fig. 9. Number of unknows in thousands (TSD), $\boldsymbol{T}$-formulations.

BC for $\boldsymbol{T}_2$ for $\boldsymbol{T}$-formulations, which is exact for the MS-FEM approaches (17) and (18), respectively. However, an additional term for $\boldsymbol{A}$-formulations in the MSFEM approaches is required, the third term in (19) and (20), respectively, which is an approximation only.

E. Computational Costs

The number of required unknowns are presented in Figs. 9 and 10. The FEO of the methods and their

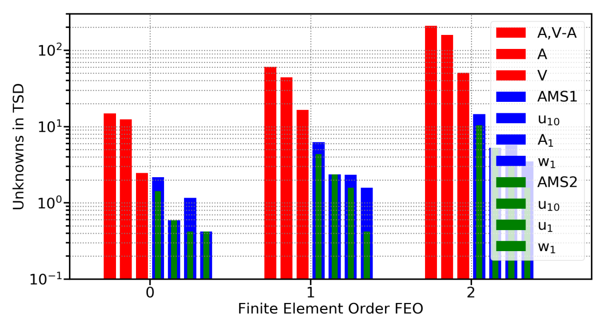

Fig. 10. Number of unknows in thousands (TSD), $\boldsymbol{A}$-formulations.

This article has been accepted for publication in IEEE Transactions on Energy Conversion. This is the author's version which has not been fully edited and content may change prior to final publication. Citation information: DOI 10.1109/TEC.2023.3333530

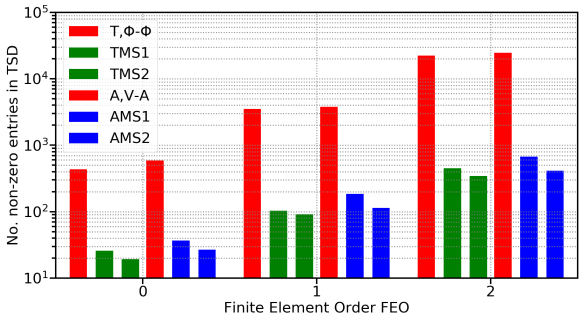

Fig. 11. Non-zero entries in finite element matrix.

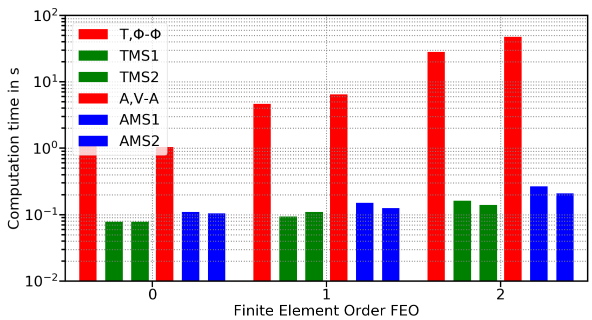

Fig. 12. Computation time, half problem.

potentials are summarized in Tab. I. In general, the 2D/1D MSFEMs require essentially less unknowns than the 3D FEMs, about a factor of 10. A significant additional reduction of the unknowns by the 2D/1D MSFEMs can be obtained by replacing $\boldsymbol{T}_0$ and $\boldsymbol{A}_1$ by $\operatorname{grad}\Phi_0$ and $\operatorname{grad} u_1$, respectively. To be fair the 3D FEMs could exploit the symmetry with respect to the plane z=0.

The memory requirement is reflected by means of the non-zero entries in Fig. 11. Memory requirements increase visibly less rapidly for 2D/1D MSFEMs and are at least 10 times smaller than for 3D FEMs.

TMS2 needs less unknowns and less non-zero entries in the FE-system than TMS1. The same can be stated for AMS2 and AMS1.

The computation times (CTs) presented in Figs. 12 and 13 consist of the solution of the problem including the evaluation of eddy current losses P and P_{EE}. In general, $\boldsymbol{A}$-formulations require more computation time than $\boldsymbol{T}$-formulations and obviously AMS1 requires more computation time than AMS2. The CTs and their increase from the half to the entire problem with respect to the FEO of the 3D reference solutions are essentially higher than those of the 2D/1D-MSFEM problems. Overall, the 2D/1D MSFEMs are more than 100 times faster than the 3D FEMs for second order FEO.

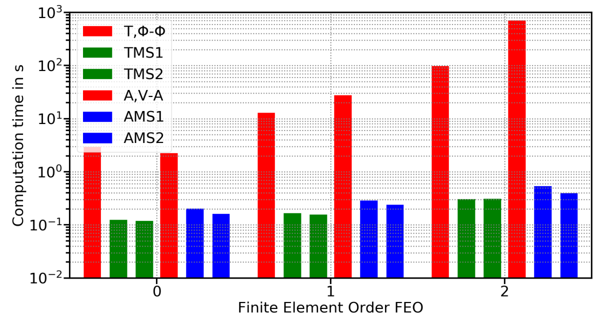

Fig. 13. Computation time, entire problem.

F. Frequency Sweeps

Some frequency sweeps of EC losses have been investigated to show the robustness of the 2D/1D MSFEMs with respect to the penetration depth

$$\delta = \sqrt{\frac{2}{\omega\mu\sigma}}. \tag{69}$$

The frequency range of 50 to 6,400 Hz was selected, which means penetration depths of 1.561mm to 0.138mm. All simulations are based on half problems and FEO=2.

The behavior of the EC losses as a function of δ/d is shown in Fig. 14 and the behavior of the losses due to EE is shown in Fig. 15. The overall EC losses obtained by TMS1 and TMS2 are essentially more accurate than those by AMS1 and AMS2 as can be seen in Fig. 16. The relatively large error at small penetration depths in Fig. 17 is due to the rather coarse FE mesh in the xy-plane along the edges, compare with Fig. 1. The relative errors of TMS1 and TMS2 are related to $\boldsymbol{T}$,Φ-Φ and of AMS1 and AMS2 to $\boldsymbol{A}$,V-$\boldsymbol{A}$.

In summary, TMS1 and TMS2 are significantly more accurate than AMS1 and AMS2. To cope also for higher frequencies, i.e. $\delta/d \ll 1$, the approaches (17) to (20) have to be extended to approaches of higher order 2D/1D MSFEMs. Principal ideas to this end can be found in [6] and [21].

G. Solving the Equation Systems of 2D/1D MSFEMs

The solvability of the equation systems resulting from 2D/1D MSFEMs and the performance of different solvers in case of FEO=2 are presented here. One half of the segment was considered, see Fig. 1. The direct solvers, the parallel direct solver (PARDISO) [20], the sparse Cholesky solver (SCS) [22] and the unsymmetric multifrontal package (UMPFPACK) [23] and the iterative solver conjugate gradient method (CGM) with the preconditioner balancing domain decomposition by

This article has been accepted for publication in IEEE Transactions on Energy Conversion. This is the author's version which has not been fully edited and content may change prior to final publication. Citation information: DOI 10.1109/TEC.2023.3333530

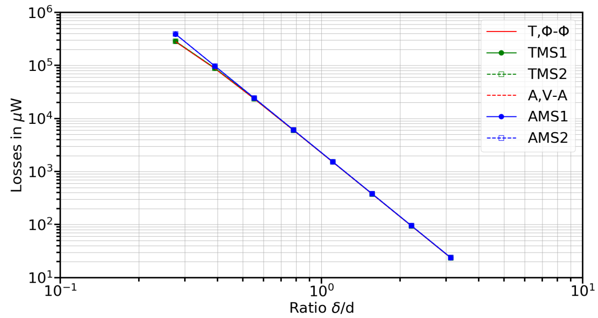

Fig. 14. Eddy current losses, half problem, FEO=2 see Tab. I.

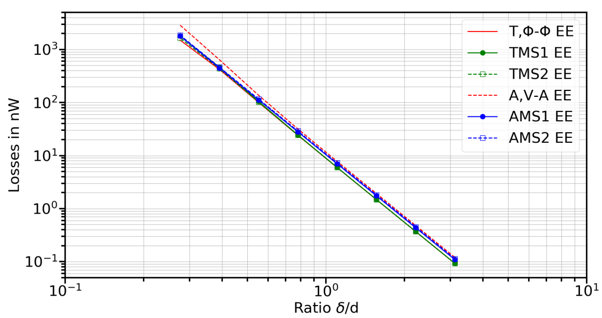

Fig. 15. Eddy current losses of EE, half problem, FEO=2 see Tab. I.

constraints (BDDC) [24] and with block Jacobi preconditioning (BJPC) [22] were studied.
To evaluate mainly the iterative solvers the residual

$$\mathbf{r} = \mathbf{b} - \mathbf{A}\mathbf{x} \tag{70}$$

of the equation system $A\mathbf{x} = \mathbf{b}$ with the matrix A, the vector of degrees of freedom $\mathbf{x}$ and the right hand side $\mathbf{b}$ is used to define the reduction factor

$$f_r = \frac{\|\mathbf{r}\|_2}{\|\mathbf{r_0}\|_2} \tag{71}$$

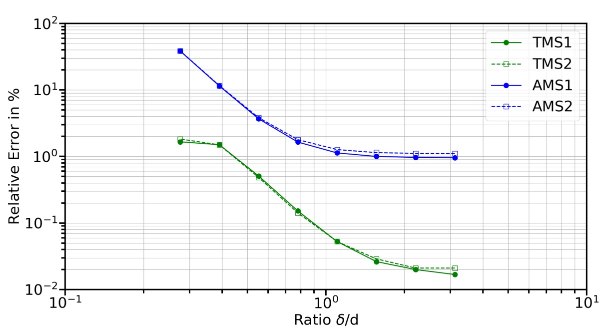

Fig. 16. Relative error of eddy current losses, half problem, FEO=2 see Tab. I.

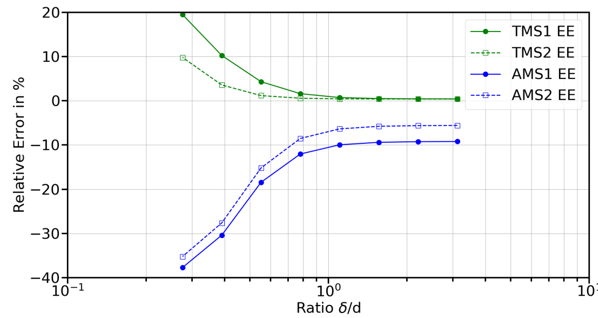

Fig. 17. Relative error of eddy current losses of EE, half problem, FEO=2 see Tab. I.

based on the initial residual $\mathbf{r_0}$.
"Usable", "inaccurate" and "wrong" were chosen in order to make a more differentiated evaluation of the results. Investigations show that a rather moderate small value $f_r < 10^{-4}$ already leads to useful losses using an iterative solver, compare CGM with BDDC and TMS1 and TMS2. The maximum number of iterations was chosen generously with 100 in order to see if a solver can in principle deliver a feasible result.
PARDISO is the only solver that solves all problems including the reference problems reliably and, thus allows a fair comparison. For this reason, PARDISO was selected for all investigations above in Secs. V-B to Sec. V-F.
SCS is the fastest solver for the 2D/1D MSFEMs. UMPFPACK clearly takes more time than PARDISO. CGM with BJPC always fails, whereas CGM with BDDC is fast and provides feasible solutions.
Quite similar conclusions can be drawn with FEO=1, except that the results of AMS1 are slightly better than those of AMS2. However, this is not presented here.

VI. Conclusions

The approaches for 2D/1D MSFEMs are quite similar to those for 3D MSFEMs [16], [17]. While the coefficient functions for 2D/1D MSFEMs depend on two variables, those for 3D depend on three variables. Note, the term $\phi_1^0 \operatorname{grad} u_{10}$ in (19) and (20) is not suitable in 3D.
Losses obtained by 2D/1D MSFEMs differ from the reference losses by less than about one percent. The MSFEMs with $\boldsymbol{T}$-formulations are noticeably more accurate than MSFEMs with $\boldsymbol{A}$-formulations.
The 2D/1D MSFEMs are accurate for penetration depths δ with $\delta/d \geq 1$, TMS1 and TMS2 provide accurate results even for clearly smaller δ.
Overall, the number of unknowns for the 2D/1D MSFEMs is much smaller than that for the 3D FEMs. Simulations with 2D/1D MSFEMs are much faster than those with 3D FEMs.

The 2D/1D MSFEMs are able to handle problems with complicated geometries, Biot-Savart fields, symmetries and the EE.

Application of the proposed methods to the time domain or to nonlinear problems is obviously possible.

An available 2D FE code supporting H^1 and $H(curl)$ FEs allows in principle the implementation of the presented 2D/1D MSFEMs. The MSFEM approach (20) requires only H^1 FEs.

Direct solvers are suitable to reliably solve systems of equations from 2D/1D MSFEMs. CGM with BDDC is a feasible iterative solver. A specific pre-conditioner for 2D/1D MSFEMs would be helpful for large problems. The development of a tailored preconditioner for 2D/1D MSFEMs would be interesting to see if a better performance can be achieved.

The use of 2D/1D MSFEMs is a very attractive alternative to both brute force 3D FEMs and 2D/1D methods.

Acknowledgment

This work was supported by the Austrian Science Fund (FWF) under projects P 31926.

References

[1] P. Handgruber, A. Stermecki, O. Bíró, A. Belahcen, and E. Dlala, "Three-Dimensional Eddy-Current Analysis in Steel Laminations of Electrical Machines as a Contribution for Improved Iron Loss Modeling," *IEEE Trans. Ind. Appl.*, vol. 49, no. 5, pp. 2044–2052, Sept 2013.

[2] M. Schöbinger, I. Tsukerman, and K. Hollaus, "Effective Medium Transformation: The Case of Eddy Currents in Laminated Iron Cores," *IEEE Trans. Magn.*, vol. 57, no. 11, pp. 1–6, 2021.

[3] O. Bottauscio and M. Chiampi, "Analysis of laminated cores through a directly coupled 2-D/1-D electromagnetic field formulation," *IEEE Trans. Magn.*, vol. 38, no. 5, pp. 2358–2360, 2002.

[4] J. Pippuri and A. Arkkio, "Time-Harmonic Induction-Machine Model Including Hysteresis and Eddy Currents in Steel Laminations," *IEEE Trans. Magn.*, vol. 45, no. 7, pp. 2981–2989, 2009.

[5] C. Geuzaine, S. Steentjes, K. Hameyer, and F. Henrotte, "Pragmatic two-step homogenisation technique for ferromagnetic laminated cores," *IET Meas. Sci. Technol.*, vol. 9, no. 2, pp. 152–159, 2015.

[6] K. Hollaus and J. Schöberl, "Some 2-D Multiscale Finite-Element Formulations for the Eddy Current Problem in Iron Laminates," *IEEE Trans. Magn.*, vol. 54, no. 4, pp. 1–16, April 2018.

[7] K. Hollaus and M. Schöbinger, "Air Gap and Edge Effect in the 2-D/1-D Method With the Magnetic Vector Potential A Using MSFEM," *IEEE Trans. Magn.*, vol. 56, no. 1, pp. 1–5, Jan 2020.

[8] L. Vandenbossche, S. Jacobs, F. Henrotte, and K. Hameyer, "Impact of cut edges on magnetization curves and iron losses in e-machines for automotive traction," *World Electric Vehicle Journal*, vol. 4, no. 3, pp. 587–596, 2010. [Online]. Available: https://www.mdpi.com/2032-6653/4/3/587

[9] M. Bali and A. Muetze, "Modeling the Effect of Cutting on the Magnetic Properties of Electrical Steel Sheets," *IEEE Transactions on Industrial Electronics*, vol. 64, no. 3, pp. 2547–2556, 2017.

[10] R. Sundaria, D. G. Nair, A. Lehikoinen, A. Arkkio, and A. Belahcen, "Effect of Laser Cutting on Core Losses in Electrical Machines-Measurements and Modeling," *IEEE Transactions on Industrial Electronics*, vol. 67, no. 9, pp. 7354–7363, 2020.

[11] P. Rasilo, E. Dlala, K. Fonteyn, J. Pippuri, A. Belahcen, and A. Arkkio, "Model of laminated ferromagnetic cores for loss prediction in electrical machines," *IET Electric Power Applications*, vol. 5, no. 7, pp. 580–588, August 2011.

[12] M. Schöbinger, J. Schöberl, and K. Hollaus, "Multiscale FEM for the Linear 2-D/1-D Problem of Eddy Currents in Thin Iron Sheets," *IEEE Tran. Magn.*, vol. 55, no. 1, pp. 1–12, Jan 2019.

[13] K. Hollaus and M. Schöbinger, "Multiscale Finite Element Formulations for 2D/1D Problems," in *2022 IEEE 20th Biennial Conference on Electromagnetic Field Computation (CEFC)*, 2022, pp. 1–2.

[14] R. Stoll, *The analysis of eddy currents*, ser. Monographs in electrical and electronic engineering. Oxford University Press, 1974.

[15] J. Schöberl and S. Zaglmayr, "High order Nédélec elements with local complete sequence properties," *COMPEL*, vol. 24, no. 2, pp. 374–384, 2005.

[16] K. Hollaus, "A MSFEM to Simulate the Eddy Current Problem in Laminated Iron Cores in 3D," *COMPEL*, vol. 38, no. 5, pp. 1667–1682, 2019.

[17] K. Hollaus and M. Schöbinger, "A Multiscale FEM for the Eddy Current Problem with $\boldsymbol{T}$, Φ - Φ in Laminated Conducting Media," *IEEE Trans. Magn.*, pp. 1–4, 2020.

[18] O. Bíró, "Edge element formulations of eddy current problems," *Comput. Methods Appl. Mech. Engrg.*, vol. 169, no. 3-4, pp. 391–405, 1999.

[19] J. Schöberl. NetGen/NGSolve. [Online]. Available: https://ngsolve.org

[20] O. Schenk and K. Gärtner, *PARDISO*. Boston, MA: Springer US, 2011, pp. 1458–1464.

[21] K. Hollaus and J. Schöberl, "A Higher Order Multi-Scale FEM with A for 2D Eddy Current Problems in Laminated Iron," *IEEE Trans. Magn.*, vol. 51, no. 3, 2015.

[22] Y. Saad, *Iterative Methods for Sparse Linear Systems*, 2nd ed. Society for Industrial and Applied Mathematics, 2003.

[23] T. A. Davis, "Algorithm 832: UMFPACK V4.3—an Unsymmetric-Pattern Multifrontal Method," *ACM Trans. Math. Softw.*, vol. 30, no. 2, pp. 196–199, jun 2004.

[24] C. R. Dohrmann, "A Preconditioner for Substructuring Based on Constrained Energy Minimization," *SIAM Journal on Scientific Computing*, vol. 25, no. 1, pp. 246–258, 2003.

This article has been accepted for publication in IEEE Transactions on Energy Conversion. This is the author's version which has not been fully edited and content may change prior to final publication. Citation information: DOI 10.1109/TEC.2023.3333530

APPENDIX A

TABLE III
SOLVING THE EQUATION SYSTEMS

Formulation	Solver	Pre-Cond.	P (μW)	P_E (nW)	No. Iterations	Simul.-Time (s)	f_r	Result
$\mathbf{T}$,Φ-Φ	PARDISO	-	23.82	92.55	1	30.32	$1.41 \cdot 10^{-7}$	reference
	UMPFPACK		singular, no result					
	SCS							
	CGM	BJPC						
	CGM	BDDC						
$\mathbf{A}$,V-$\mathbf{A}$	PARDISO	-	23.69	120.4	1	47.17	$3.75 \cdot 10^{-8}$	reference
	UMPFPACK		singular, no result					
	SCS							
	CGM	BJPC						
	CGM	BDDC						
TMS1	PARDISO	-	23.82	92.95	1	0.202	$1.13 \cdot 10^{-6}$	usable
	UMPFPACK		23.82	92.95	1	1.574	$6.89 \cdot 10^{-8}$	usable
	SCS		23.82	92.95	1	0.156	$8.21 \cdot 10^{-8}$	usable
	CGM	BJPC	5,293	23,733	100	0.187	$9.0 \cdot 10^{-3}$	wrong
	CGM	BDDC	23.81	92.78	17	0.187	$9.25 \cdot 10^{-5}$	usable
TMS2	PARDISO	-	23.82	92.92	1	0.141	$1.39 \cdot 10^{-13}$	usable
	UMPFPACK		23.82	92.92	1	0.453	$6.19 \cdot 10^{-15}$	usable
	SCS		23.82	92.92	1	0.156	$2.64 \cdot 10^{-14}$	usable
	CGM	BJPC	1,906	45,036	100	0.172	$2.01 \cdot 10^{-2}$	wrong
	CGM	BDDC	23.81	92.75	17	0.141	$9.25 \cdot 10^{-5}$	usable
AMS1	PARDISO	-	23.92	109.3	1	0.375	$3.92 \cdot 10^{-13}$	inaccurate
	UMPFPACK		23.92	109.3	1	0.942	$4.26 \cdot 10^{-14}$	inaccurate
	SCS		23.92	109.3	1	0.266	$1.16 \cdot 10^{-13}$	inaccurate
	CGM	BJPC	53.91	2,283	100	0.320	1.56	wrong
	CGM	BDDC	23.92	109.3	43	0.344	$8.9 \cdot 10^{-5}$	inaccurate
AMS2	PARDISO	-	23.95	113.7	1	0.187	$8.9 \cdot 10^{-12}$	usable
	UMPFPACK		23.95	113.7	1	0.656	$2.67 \cdot 10^{-12}$	usable
	SCS		23.95	113.7	1	0.219	$7.52 \cdot 10^{-12}$	usable
	CGM	BJPC	79.96	10,723	100	0.217	2.11	wrong
	CGM	BDDC	23.95	113.7	40	0.219	$5.34 \cdot 10^{-5}$	usable

BDDC balancing domain decomposition by constraints
BJPC block Jacobi preconditioning
CGM conjugate gradient method
f_r reduction of the residual, see (71)
PARDISO parallel direct solver
SCS sparse Cholesky solver
UMPFPACK unsymmetric multifrontal package